Geophys. J. Int. (2008) **173,** 157–167 doi: 10.1111/j.1365-246X.2007.03581.x

SH-waves scattering from a partially filled semi-circular alluvial valley

Deng-How Tsaur and Kao-Hao Chang

Department of Harbor and River Engineering, National Taiwan Ocean University, No. 2, *Beining Rd., Keelung* 202-24, *Taiwan.*
E-mail: hretdh@mail.ntou.edu.tw

Accepted 2007 August 6. Received 2007 June 23; in original form 2007 April 23

SUMMARY

A series solution of the plane SH-waves incident on a partially filled semi-circular alluvial valley imbedded in a half-space is presented. Based on the region-matching method, the analysed region is decomposed into two subregions by the interface between two media. The antiplane displacement field of each subregion is expressed in terms of an infinite series of cylindrical wavefunctions with unknown expansion coefficients. After imposing the traction-free condition on the curved valley surface and the matching conditions on the interface with the aid of Graf's addition theorem, the unknown coefficients are obtained. Both the frequency- and time-domain responses are evaluated. In the theoretical derivation of this work, two classical exact series solutions are also included, so the present series solution is more general than those given before. Visible effects of different physical parameters on ground surface motions are illustrated in graphical form.

Key words: Earthquake ground motions; Site effects; Wave scattering and diffraction.

1 INTRODUCTION

Analysis of local site effects is an important component of earthquake hazard assessment and microzonation. The geological and surface soil conditions of a region contribute in the determination of how much the ground will shake. For a long time, field observations following large earthquakes or records of the same events have shed substantial light on the seismological, geological and structural aspects of these effects. From various works, it is well established that alluvial valleys and sedimentary basins are prone to much stronger ground shaking than bedrock, and these site amplifications can vary rapidly from place to place. Furthermore, signal records on such sites are longer and more complex than those on well-cemented sandstones or crystalline rocks. Consequently, better understanding of the mechanism of these amplification phenomena provides crucial information for earthquake disaster mitigation and the design of earthquake resistant structures.

As to the partially filled alluvial valley, it is a kind of 'more realistic' alluvial valley. Its cross-section shape is very similar to those of Chusal and Runo valleys in Garm region (former USSR). Chusal Valley is, about 700 m long, 400 m wide and 60 m deep, located in the Tien Shan Mountains, while Runo Valley is, about 5 km long, 700 m wide and 100 m deep, seated in the Pamir Mountains (Tucker & King 1984). In 1984 King and Tucker performed an instrumental study of the response to earthquake motion of these two valleys. Indeed, this type of cross-section shape has caught our eyes. Although it seems to be very simple, the separation of variables still cannot be applied directly due to its nature of shape involving both circular-arc and straight boundaries. So far, its exact solution is extremely difficult to obtain.

Over the past three decades, the two-dimensional (2-D) half-plane scattering problems of local geological structures or topography have been pursued. Nowadays, it is believed that the effects of local alluvium thickness on seismic motions exist and can be significant (e.g. Hudson 1972; Bard & Bouchon 1980). Referring to the complex models (e.g. irregular valleys with heterogeneous materials), numerical approximation methods are, no doubt, the most convenient and powerful tools to tackle these subjects. The most widely used include the finite difference method (FDM) (e.g. Boore 1972), the finite element method (FEM) (e.g. Lysmer & Drake 1972; Smith 1975; Bielak *et al.* 1999), and the boundary element method (BEM) (e.g. Papageorgiou & Kim 1991; Sánchez-Sesma *et al.* 1993; Fishman & Ahmad 1995; Luzón *et al.* 2004). Also, the BEM can be coupled with the FEM (e.g. Bielak *et al.* 1991) or the discrete wavenumber method (e.g. Bouchon *et al.* 1989; Kawase & Aki 1989; Gil-Zepeda *et al.* 2003).

Among the above-mentioned approaches, each one has its limitation. The FDM and FEM have the disadvantage that they need to fill the entire domain with mesh grids. So, it is not uncommon for these domain methods to require considerable computational time and large memory supercomputers. Moreover, another drawback of them is on the introduction of an artificial boundary, on which one must specify an approximate radiation condition to eliminate spurious wave reflections. As a result, using them is not feasible for large dimension problems. By contrast, the BEM has gained increasing popularity. Its main attributes are: (1) it maps the domain equation on the boundary and thus reduces the problem dimension by one, (2) there is no need to choose a fictitious boundary because of the relatively easy fulfilment of radiation conditions at infinity and (3) qualities of interest can be calculated at any field point through

an integral representation. Nevertheless, if the material fillings are highly heterogeneous, the application of BEM becomes cumbersome. In conclusion, despite the sophisticated numerical methods are very suitable to complicated geological configurations, the theoretical schemes are still needed and expected because they provide a quantitative check on the accuracy of numerical approximation methods. Confidence in accuracy is important for developing better approximate techniques.

Generally speaking, theoretical solutions to the scalar wave equation require the scatterer's surface to coincide with the coordinate system. In other words, only geometries that allow separation of variables (also known as the wavefunction expansion) yield complete expressions for the associated eigenfunctions. Unfortunately, in reviewing the theoretical analysis methods (e.g. series approach) in this field, such solutions (in particular exact solutions) are restricted to a few simple geometric shapes (like a circle or ellipse). Take the full-space elastodynamic inclusion problem for instance; Pao & Mow (1973) gives a comprehensive coverage of exact solutions in their monograph. As to the half-space problem involving the contrasting material properties, the representative cases are a semi-circular (Trifunac 1971) and semi-elliptical alluvial valley (Wong & Trifunac 1974).

To the authors' knowledge, the series solution to the scattering problem of plane SH waves from a partially filled semi-circular alluvial valley is not found yet. Therefore, in this paper, the authors intend to handle this issue theoretically by means of the region-matching method. The present series solution can provide not only adequate validation for other numerical solutions but also better physical insights into the problem. It may replace regret for the lack of exact solution as well.

The major contributions of this work are twofold. On one hand, the region-matching technique is successfully applied to a partially filled semi-circular alluvial valley. On the other hand, the boundary-value problem solved herein has led to the development of new series solutions for several types of partially filled semi-circular alluvial valley.

2 THEORETICAL FORMULATION

The 2-D model depicted in Fig. 1 consists of an infinitely long, partially filled, alluvial valley embedded into a semi-infinite medium. The valley cross-section is basically semi-circular in shape (with radius a), but the sediment is horizontally deposited at the bottom.

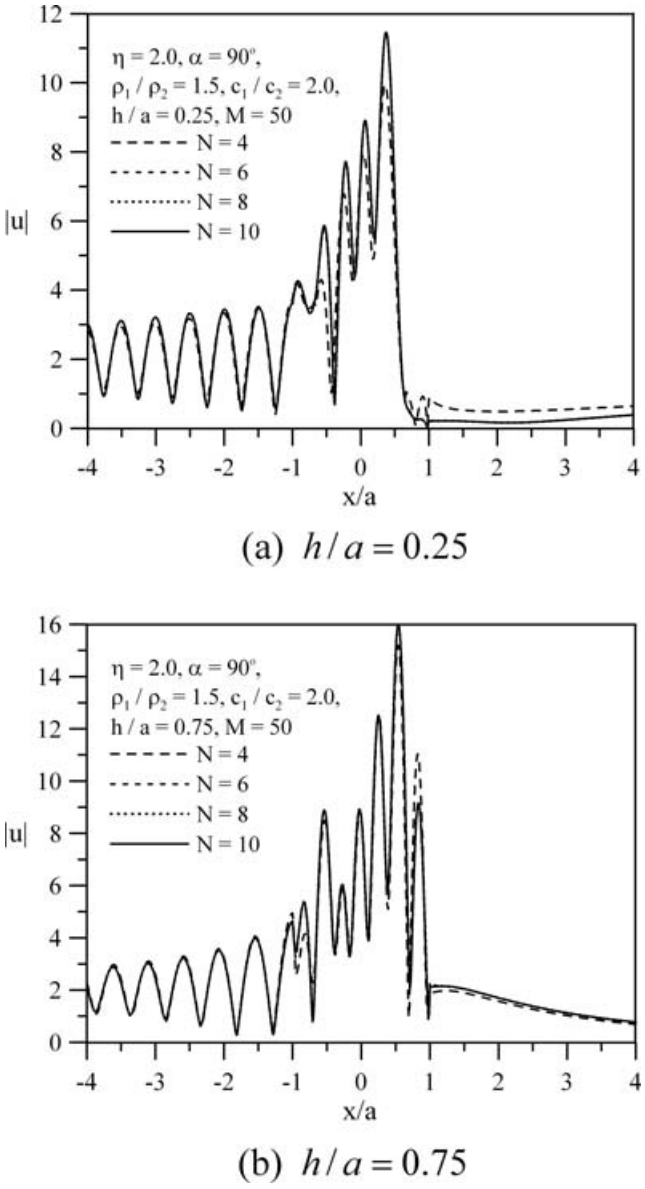

Figure 2. Displacement amplitudes versus x/a for different values of N at $\eta = 2.0$ and $\alpha = 90°$.

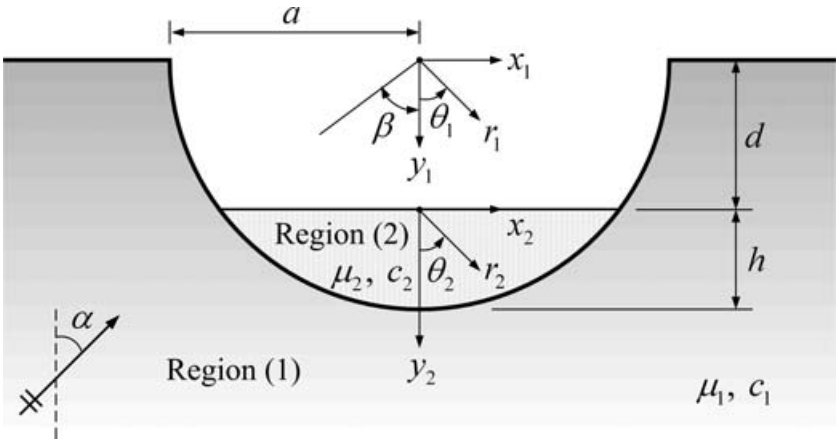

Figure 1. Geometry of the problem.

The thickness and central angle of the alluvium are h and 2β, respectively. The vertical distance from top surface of the deposit to flat ground surface is d. The contact interface between the half-space and the alluvium is supposed to be perfectly bonded. All material properties involved are assumed to be isotropic, homogeneous and linearly elastic. The shear modulus, mass density and shear wave velocity are given by μ, ρ and $c = \sqrt{\mu/\rho}$, respectively. The subscripts, 1 and 2, designate these constants in the half-space and the deposit, respectively. The definitions of two Cartesian and two cylindrical coordinate systems are taken as shown in Fig. 1. The origin of global coordinate systems (x_1, y_1) and (r_1, θ_1) is set at the centre of curvature of the valley, and the origin of local coordinate systems (x_2, y_2) and (r_2, θ_2) is located at the centre of the top surface of the alluvium. In both Cartesian coordinate systems, the horizontal axes are defined as positive going to the right direction, while the vertical axes are defined as positive going downward. In two cylindrical coordinate systems, θ_1 and θ_2 are measured counter-clockwise from the positive vertical axes. An infinite train of plane SH waves of unit amplitude, which impinges on the valley at an angle α to the negative y-axis, is considered.

Concerning the mass density ratio and shear wave velocity ratio, if they are greater than one, it means that the alluvial filling is relatively softer than the surrounding half-space (e.g. clay, silty or sandy layers lying directly on crystalline rock). On the contrary, if these two ratios are smaller than one, it implies that the filling material in the valley is relatively harder than that outside the valley.

As seen in Fig. 1, the interface divided the half-space into two subregions, a semi-unbounded outer region (1) and a bounded inner region (2). In both regions the steady-state out-of-plane motions, by exciting the valley with an incident plane SH wave, are required to satisfy the governing wave equations, namely

$$\nabla^2 U_j = \frac{1}{c_j^2}\frac{\partial^2 U_j}{\partial t^2}, \quad j = 1, 2, \tag{1}$$

where ∇^2 is the 2-D cylindrical Laplacian, $U_j = u_j \exp(i\omega t)$ represents the displacement field, u_j is the spatial function, i is $\sqrt{-1}$, ω is the angular frequency, and t is the time variable. Substituting $u_j \exp(i\omega t)$ into eq. (1), the wave equations turn out to be Helmholtz equations as follows

$$\nabla^2 u_j + k_j^2 u_j = 0, \quad j = 1, 2, \tag{2}$$

where $k_j = \omega/c_j$ is shear wavenumber. The time-harmonic factor $\exp(i\omega t)$ is suppressed henceforth in all the expressions throughout this paper.

The zero-stress boundary conditions on the ground surface, the curved surface of the valley and on the top surface of the deposit are

$$\tau^{(1)}_{\theta_1 z} = \frac{\mu_1}{r_1}\frac{\partial u_1}{\partial \theta_1} = 0, \quad \theta_1 = \pm\pi/2, \quad r_1 > a \tag{3}$$

$$\tau^{(1)}_{r_1 z} = \mu_1 \frac{\partial u_1}{\partial r_1} = 0, \quad \beta \le |\theta_1| \le \pi/2, \quad r_1 = a \tag{4}$$

$$\tau^{(2)}_{\theta_2 z} = \frac{\mu_2}{r_2}\frac{\partial u_2}{\partial \theta_2} = 0, \quad \theta_2 = \pm\pi/2, \quad r_2 \le a\sin\beta. \tag{5}$$

In addition, two matching conditions along the interface between region (1) and (2), which assure the continuity of displacement and stress fields, requires

$$u_1(a, \theta_1) = u_2(a, \theta_1), |\theta_1| \le \beta \tag{6}$$

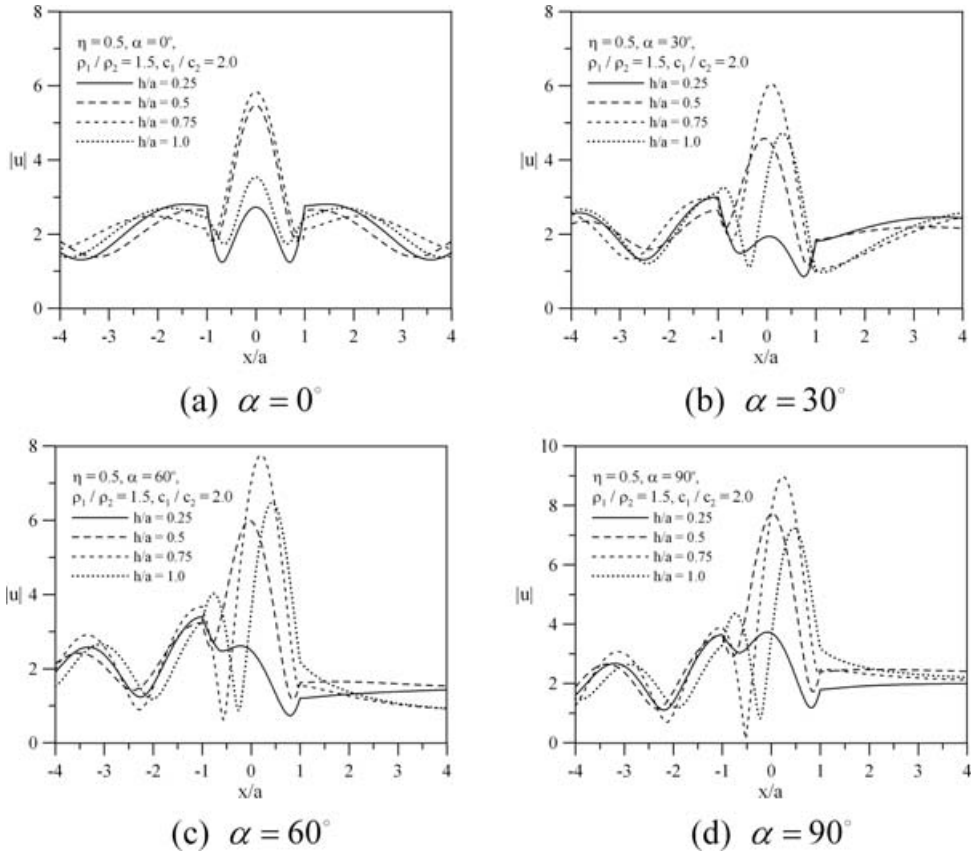

Figure 3. Displacement amplitudes versus x/a for different h/a at $\eta = 0.5$, $\rho_1/\rho_2 = 1.5$ and $c_1/c_2 = 2.0$.

$$\tau^{(1)}_{r_1z}(a,\theta_1) = \tau^{(2)}_{r_1z}(a,\theta_1),\ |\theta_1| \le \beta. \tag{7}$$

In semi-unbounded region (1), the incident wavefield $u^I(r_1,\theta_1)$ and the reflected wavefield $u^R(r_1,\theta_1)$ can be expressed as

$$u^I(r_1,\theta_1) = \exp[ik_1r_1\cos(\theta_1+\alpha)] \tag{8}$$

$$u^R(r_1,\theta_1) = \exp[-ik_1r_1\cos(\theta_1-\alpha)]. \tag{9}$$

Employing a distinguished formula (see Abramowitz & Stegun 1972), an expansion for the exponential in terms of Bessel functions is as follows

$$\exp(\pm ik_1r_1\cos\theta_1) = \sum_{n=0}^{\infty}\bar{\delta}_{0n}(\pm i)^nJ_n(k_1r_1)\cos n\theta_1, \tag{10}$$

where $\bar{\delta}_{0n} = 2-\delta_{0n}$, δ_{0n} is the Kronecker delta function, and $J_n(\cdot)$ denotes the Bessel function of the first kind of order n.

Substituting eq. (10) into eqs (8) and (9), respectively, and then adding them together, the free field displacement $u^F(r_1,\theta_1)$ can be written as

$$u^F(r_1,\theta_1) = 2\sum_{n=0}^{\infty}\bar{\delta}_{0n}(-1)^nJ_{2n}(k_1r_1)\cos(2n)\alpha\cos(2n)\theta_1 - 4i\sum_{n=0}^{\infty}(-1)^nJ_{2n+1}(k_1r_1)\sin(2n+1)\alpha\sin(2n+1)\theta_1. \tag{11}$$

Note that this expression automatically satisfies the boundary condition (eq. 3) on the ground surface, that is, the shear stress perpendicular to θ_1 vanishes.

Considering the scattered wavefield in region (1), it can be expended into series of cylindrical wavefunctions satisfying the Helmholtz equation (eq. 2), the stress-free boundary condition (eq. 3) and the Sommerfeld radiation condition at infinity. So, the wavefunction expansion for the scattered wavefield $u^S(r_1,\theta_1)$ is as follows

$$u^S(r_1,\theta_1) = \sum_{n=0}^{\infty}A_nH^{(2)}_{2n}(k_1r_1)\cos(2n)\theta_1 + \sum_{n=0}^{\infty}B_nH^{(2)}_{2n+1}(k_1r_1)\sin(2n+1)\theta_1, \tag{12}$$

where $H^{(2)}_n(\cdot)$ is Hankel function of the second kind of order n, and the complex expansion coefficients A_n and B_n are unknown. The physical meaning of eq. (12) is easily understood, that is, the outgoing waves radiating outward to infinity due to the presence of an alluvial valley.

The displacement of the resultant wavefield $u_1(r_1,\theta_1)$ in region (1), which is the combination of the free wavefield $u^{\mathrm{F}}(r_1,\theta_1)$ and the scattered wavefield $u^{\mathrm{S}}(r_1,\theta_1)$, can be expressed as

$$u_1(r_1,\theta_1) = u^{\mathrm{F}}(r_1,\theta_1) + u^{\mathrm{S}}(r_1,\theta_1). \tag{13}$$

Accordingly, in bounded region (2), the displacement of wavefield $u_2(r_2,\theta_2)$ satisfying the Helmholtz equation (eq. 2) and the traction-free boundary condition on the top surface of the deposit (eq. 5) is given by

$$u_2(r_2,\theta_2) = \sum_{n=0}^{\infty}C_nJ_{2n}(k_2r_2)\cos(2n)\theta_2 + \sum_{n=0}^{\infty}D_nJ_{2n+1}(k_2r_2)\sin(2n+1)\theta_2 \tag{14}$$

in which the complex expansion coefficients C_n and D_n are to be determined.

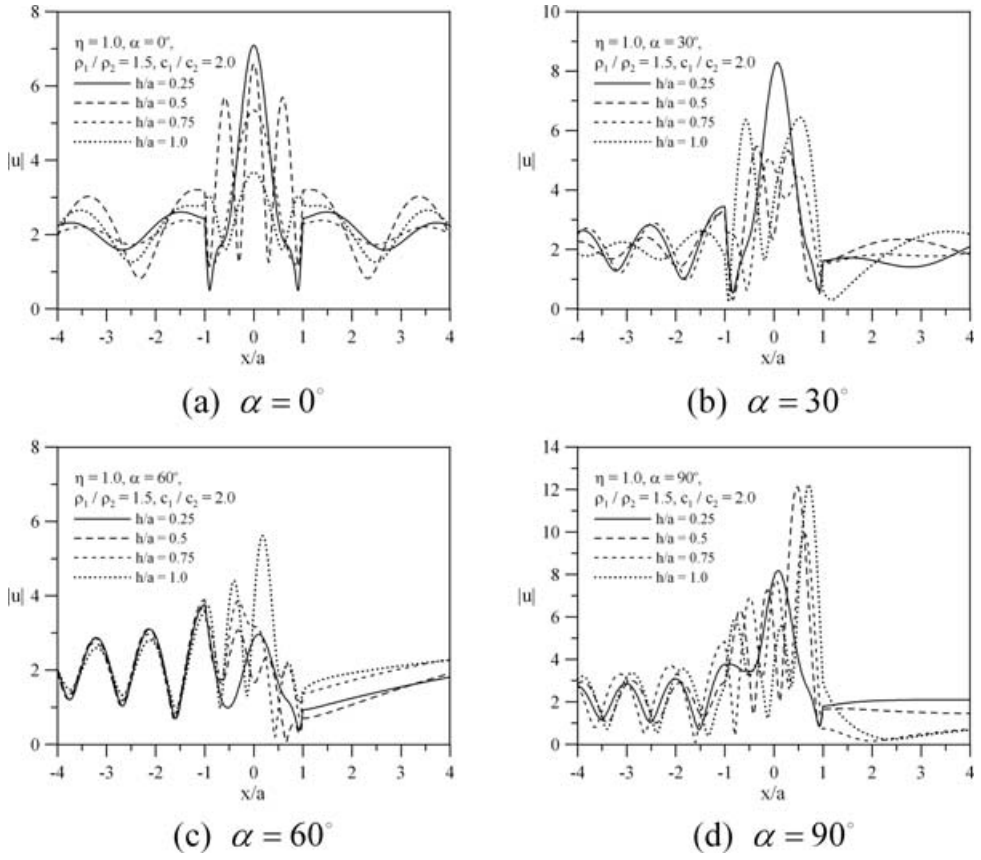

Figure 4. Displacement amplitudes versus x/a for different h/a at $\eta = 1.0$, $\rho_1/\rho_2 = 1.5$ and $c_1/c_2 = 2.0$.

Next, the core of the solution technique lies in the use of Graf's addition theorem for Bessel functions to shift the cylindrical coordinate system from (r_2, θ_2) to (r_1, θ_1). This theorem given by Watson (1958) is rewritten in a suitable form for our purposes, that is,

$$J_n(k_2 r_2)\begin{Bmatrix}\cos n\theta_2\\ \sin n\theta_2\end{Bmatrix} = (-1)^n \sum_{m=0}^{\infty} J_m(k_2 r_1)\begin{Bmatrix} J^{+}_{m,n}(k_2 d)\cos m\theta_1 \\ J^{-}_{m,n}(k_2 d)\sin m\theta_1\end{Bmatrix}, \tag{15}$$

where m and n are integers, and

$$J^{\pm}_{m,n}(k_2 d) = \frac{\bar{\delta}_{0m}}{2}[(-1)^n J_{m-n}(k_2 d) \pm J_{m+n}(k_2 d)]. \tag{16}$$

Substituting eq. (15) into (14), the displacement of wavefield in region (2) can be re-expressed as

$$u_2(r_1, \theta_1) = \sum_{n=0}^{\infty} C_n \sum_{m=0}^{\infty} J_m(k_2 r_1) J^{+}_{m,2n}(k_2 d)\cos m\theta_1 - \sum_{n=0}^{\infty} D_n \sum_{m=1}^{\infty} J_m(k_2 r_1) J^{-}_{m,2n+1}(k_2 d)\sin m\theta_1. \tag{17}$$

Applying the orthogonal properties of sine and cosine functions to the matching condition (eq. 7) and stress boundary condition (eq. 4), and integrating over the range $[-\pi/2, \pi/2]$, the following relationships for the unknown coefficients between region (1) and (2) are obtained

$$A_n = -2\bar{\delta}_{0n}(-1)^n \cos(2n)\alpha \frac{J'_{2n}(k_1 a)}{H^{(2)\prime}_{2n}(k_1 a)} + \frac{\bar{\delta}_{0n}\mu_2}{\pi H^{(2)\prime}_{2n}(k_1 a)\mu_1}\sum_{p=0}^{\infty} C_p \sum_{m=0}^{\infty} J'_m(k_2 a) J^{+}_{m,2p}(k_2 d) I^{C}_{m,2n}(\beta) \tag{18}$$

$$B_n = 4i(-1)^n \sin(2n+1)\alpha \frac{J'_{2n+1}(k_1 a)}{H^{(2)\prime}_{2n+1}(k_1 a)} - \frac{2\mu_2}{\pi H^{(2)\prime}_{2n+1}(k_1 a)\mu_1}\sum_{p=0}^{\infty} D_p \sum_{m=1}^{\infty} J'_m(k_2 a) J^{-}_{m,2p+1}(k_2 d) I^{S}_{m,2n+1}(\beta), \tag{19}$$

where the prime notation means differentiation with respect to the argument, and the functions $I^{C}_{m,n}(\beta)$ and $I^{S}_{m,n}(\beta)$ are given by

$$I^{C}_{m,n}(\beta) = \int_{-\beta}^{\beta} \cos m\theta_1 \cos n\theta_1 d\theta_1 = \begin{cases} 2\beta, & m = n = 0 \\ \beta + \dfrac{\sin(2n)\beta}{2n}, & m = n \neq 0 \\ \dfrac{\sin(m-n)\beta}{m-n} + \dfrac{\sin(m+n)\beta}{m+n}, & m \neq n \end{cases} \tag{20}$$

$$I^{S}_{m,n}(\beta) = \int_{-\beta}^{\beta} \sin m\theta_1 \sin n\theta_1 d\theta_1 = \begin{cases} \beta - \dfrac{\sin(2n)\beta}{2n}, & m = n \\ \dfrac{\sin(m-n)\beta}{m-n} - \dfrac{\sin(m+n)\beta}{m+n}, & m \neq n. \end{cases} \tag{21}$$

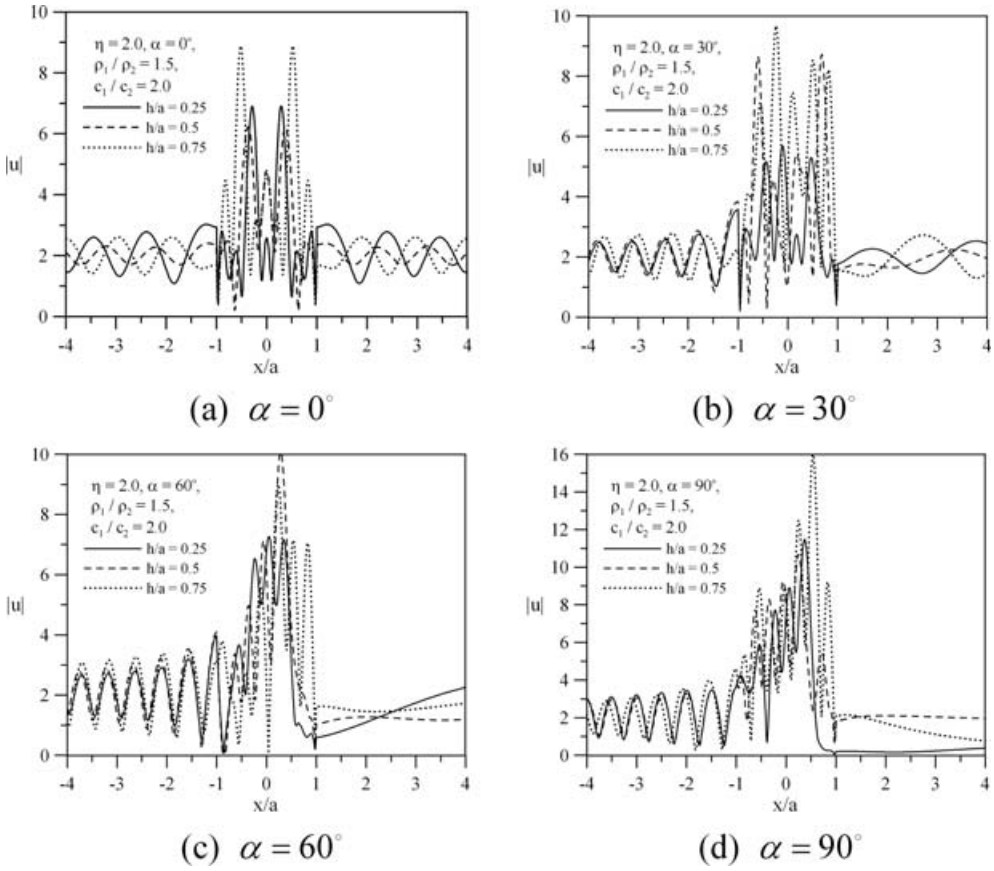

Figure 5. Displacement amplitudes versus x/a for different h/a at $\eta = 2.0$, $\rho_1/\rho_2 = 1.5$ and $c_1/c_2 = 2.0$.

Notice that the above eqs (18) and (19) are composed of two terms: the first term is related to the contribution of the empty semi-circular canyon and is consistent with the one derived by Trifunac in the early 1970s; the second term is the additional contribution of the alluvial deposit.

Similarly, utilizing the orthogonality again to the matching condition (eq. 6), and integrating over the range $[-\beta, \beta]$ results in the following infinite systems of equations,

$$2\sum_{n=0}^{\infty}\bar{\delta}_{0n}(-1)^n J_{2n}(k_1a)\cos(2n)\alpha I^C_{2n,2q}(\beta) + \sum_{n=0}^{\infty} A_n H^{(2)}_{2n}(k_1a) I^C_{2n,2q}(\beta) = \sum_{n=0}^{\infty} C_n \sum_{m=0}^{\infty} J_m(k_2a) J^+_{m,2n}(k_2d) I^C_{m,2q}(\beta), q = 0, 1, \ldots \quad (22)$$

$$-4i\sum_{n=0}^{\infty}(-1)^n J_{2n+1}(k_1a)\sin(2n+1)\alpha I^S_{2n+1,2q+1}(\beta) + \sum_{n=0}^{\infty} B_n H^{(2)}_{2n+1}(k_1a) I^S_{2n+1,2q+1}(\beta) = -\sum_{n=0}^{\infty} D_n \sum_{m=1}^{\infty} J_m(k_2a) J^-_{m,2n+1}(k_2d) I^S_{m,2q+1}(\beta), q = 0, 1, \ldots. \quad (23)$$

Taking eq. (18) into (22) and (19) into (23) to eliminate the expansion coefficients A_n and B_n, respectively, using the Wronskian relationship for the Bessel and Hankel functions (Abramowitz & Stegun 1972), and rearranging yields the following infinite systems of equations,

$$\sum_{n=0}^{\infty} C_n \sum_{m=0}^{\infty} J^+_{m,2n}(k_2d) \sum_{p=0}^{\infty} \left[J'_m(k_2a) I^C_{m,2p}(\beta) I^C_{2p,2q}(\beta) \cdot \frac{\bar{\delta}_{0p} H^{(2)}_{2p}(k_1a)\mu_2}{\pi H^{(2)\prime}_{2p}(k_1a)\mu_1} - \delta_{pq} J_m(k_2a) I^C_{m,2q}(\beta) \right] = \frac{4i}{\pi a}\sum_{n=0}^{\infty} \frac{\bar{\delta}_{0n}(-1)^n \cos(2n)\alpha I^C_{2n,2q}(\beta)}{H^{(2)\prime}_{2n}(k_1a)}, q = 0, 1, \ldots \quad (24)$$

$$\sum_{n=0}^{\infty} D_n \sum_{m=1}^{\infty} J^-_{m,2n+1}(k_2d) \sum_{p=0}^{\infty} \left[J'_m(k_2a) I^S_{m,2p+1}(\beta) I^S_{2p+1,2q+1}(\beta) \cdot \frac{2H^{(2)}_{2p+1}(k_1a)\mu_2}{\pi H^{(2)\prime}_{2p+1}(k_1a)\mu_1} - \delta_{pq} J_m(k_2a) I^S_{m,2q+1}(\beta) \right] = -\frac{8}{\pi a}\sum_{n=0}^{\infty} \frac{(-1)^n \sin(2n+1)\alpha I^S_{2n+1,2q+1}(\beta)}{H^{(2)\prime}_{2n+1}(k_1a)}, q = 0, 1, \ldots. \quad (25)$$

When one is dealing with numerical procedures, it is necessary to truncate the series in eqs (24) and (25) to a finite number (i.e. the summation indexes n and p are truncated to N terms, while the index m is truncated to M terms). The number of truncated terms, which will be taken into consideration, depends only on the accuracy requirement. After truncating the infinite series properly, the unknown coefficients C_n and D_n may be solved, respectively by standard matrix techniques. Once the unknown constants C_n and D_n are

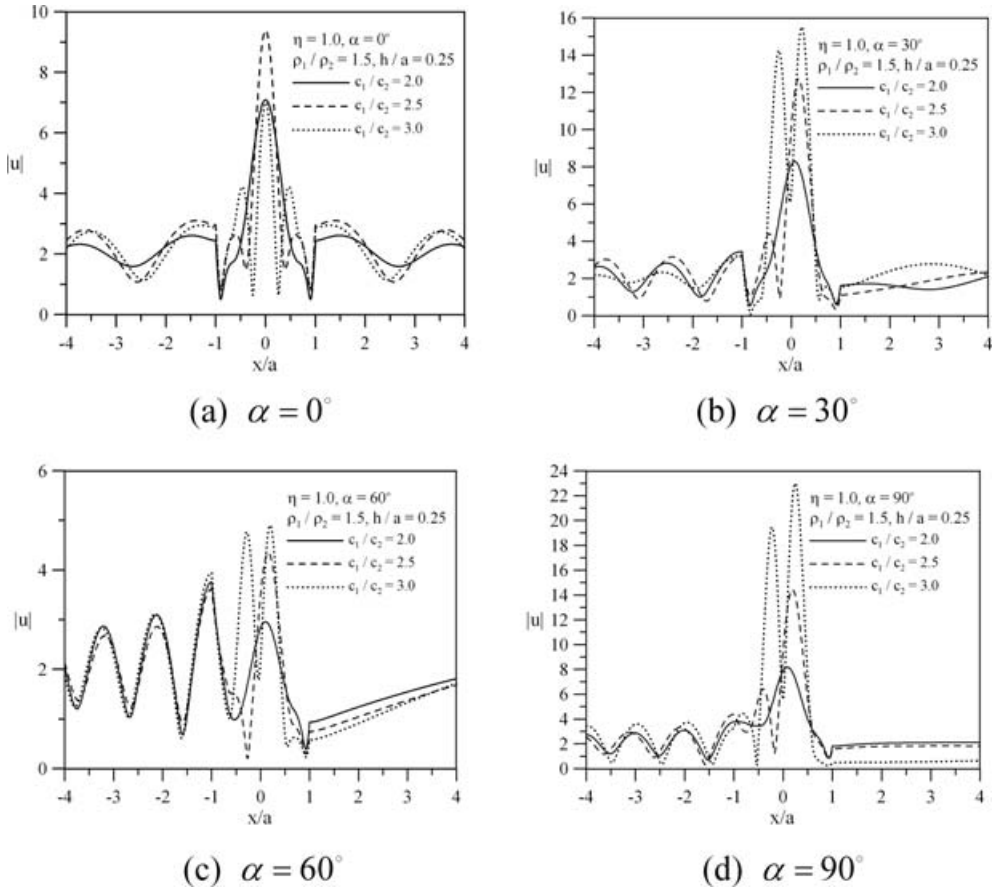

Figure 6. Displacement amplitudes versus x/a for different c_1/c_2 at $\eta = 1.0$, $\rho_1/\rho_2 = 1.5$ and $h/a = 0.25$.

obtained, it is possible to evaluate the scattering coefficients A_n and B_n by means of the truncated eqs (18) and (19) in a straightforward way.

The exact series solutions of two limiting cases may be obtained. One is the empty case when the alluvial deposit no longer exists (i.e. $d = a$ and $\beta = 0$), the problem reduces to a vacant semi-circular canyon, and the expansion coefficients A_n, B_n, C_n and D_n are derived separately as

$$A_n = -2\bar{\delta}_{0n}(-1)^n \cos 2n\alpha \frac{J'_{2n}(k_1 a)}{H^{(2)\prime}_{2n}(k_1 a)} \tag{26}$$

$$B_n = 4i(-1)^n \sin(2n+1)\alpha \frac{J'_{2n+1}(k_1 a)}{H^{(2)\prime}_{2n+1}(k_1 a)} \tag{27}$$

$$C_n = 0, \quad D_n = 0. \tag{28}$$

At a glance, one can notice that, after properly rewriting the expressions for the differentiation of Bessel and Hankel functions, eqs (26) and (27) will recover the world-renowned results of Trifunac (1973) (see his eqs 10 and 11 in page 269) except different notations are used. For this limiting case, the wavefield in region (2) must disappear as intuitively expected. In this manner, it is very clear that letting β go to zero implies that $I^C_{m,n}(0)$ and $I^S_{m,n}(0)$ go to zero also. Consequently, C_n and D_n vanish directly.

Another limiting case is when the semi-circular valley is fully filled with the alluvium (which corresponds to $d = 0$ and $\beta = \pi/2$), the unknown coefficients are obtained as

$$A_n = -2\bar{\delta}_{0n}(-1)^n \cos 2n\alpha \frac{G_{2n}}{F_{2n}} \tag{29}$$

$$B_n = 4i(-1)^n \sin(2n+1)\alpha \frac{G_{2n+1}}{F_{2n+1}} \tag{30}$$

$$C_n = \frac{-4i\bar{\delta}_{0n}(-1)^n \cos 2n\alpha}{\pi a F_{2n}} \tag{31}$$

$$D_n = \frac{-8(-1)^n \sin(2n+1)\alpha}{\pi a F_{2n+1}} \tag{32}$$

$$F_n = \mu_1 J_n(k_2 a) H^{(2)\prime}_n(k_1 a) - \mu_2 J'_n(k_2 a) H^{(2)}_n(k_1 a) \tag{33}$$

$$G_n = \mu_1 J_n(k_2 a) J'_n(k_1 a) - \mu_2 J'_n(k_2 a) J_n(k_1 a). \tag{34}$$

Once again, one can note that, after solving the famous simultaneous equations of Trifunac (1971) (see his eqs 14 and 15 in pages 1757 and 1758) and appropriately rearranging, solutions to Trifunac's equations are equivalent to eqs (29)–(32) except different symbols. Moreover, if the medium in region (2) is identical to that in region (1) (i.e. $\mu_2 = \mu_1$ and $k_2 = k_1$), G_n will go to zero and the scattering coefficients A_n and B_n will vanish immediately also. At this moment, one can obviously find that the wavefield in region (2) degenerates to be the same as the free wavefield after substituting eqs (31) and (32) back into eq. (14). In fact, the scattered waves do

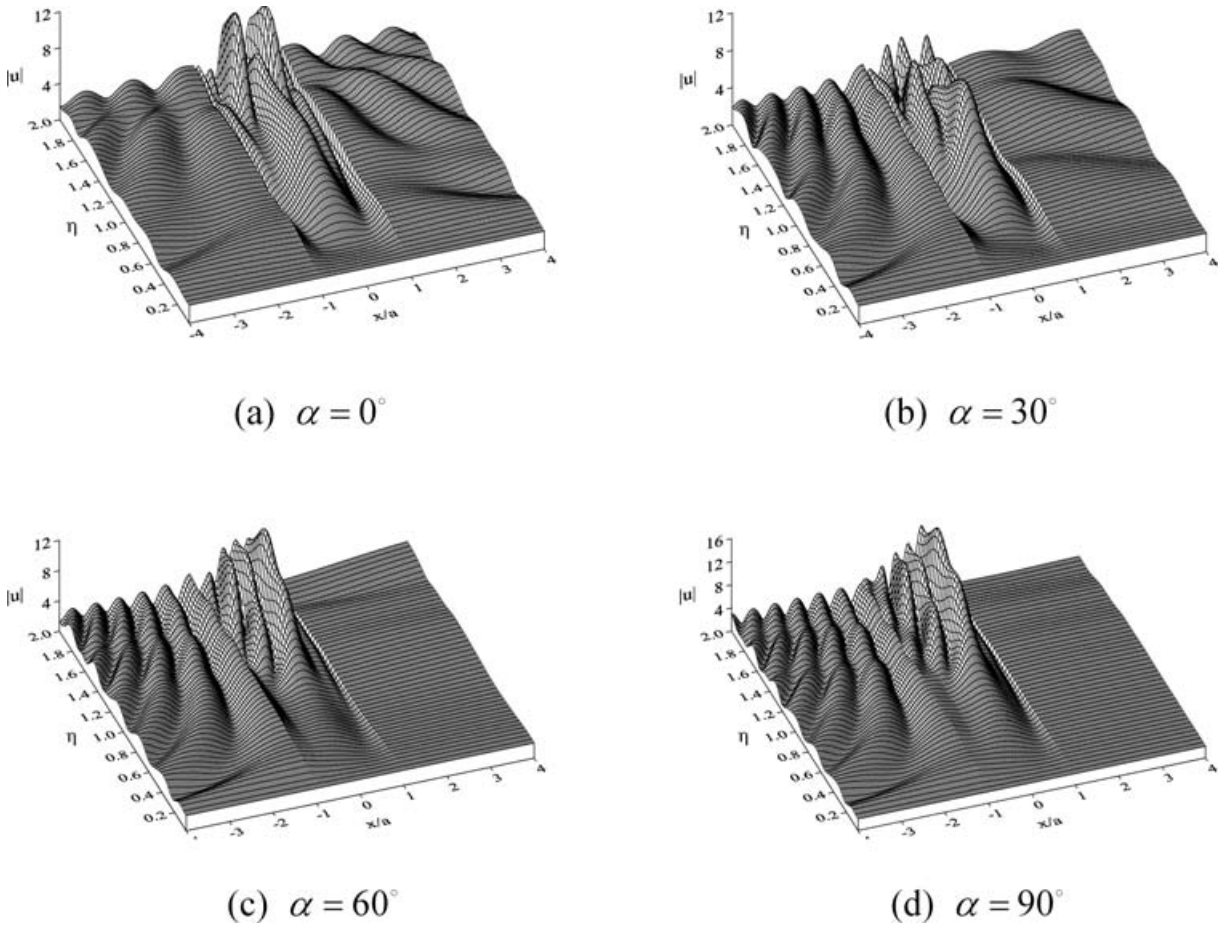

Figure 7. 3-D plots of surface displacement amplitudes for different α at $\rho_1/\rho_2 = 1.5$, $c_1/c_2 = 2.0$ and $h/a = 0.25$.

not exist any more due to the absence of the valley; in other words, only the free waves may exist in the half-space.

Returning to the partially filled case of a semi-circular alluvial valley, the displacement amplitudes is given in terms of the wave-fields by eqs (13) and (14), that is

$$|u| = \begin{cases} |u_1| = \sqrt{[\mathrm{Re}(u_1)]^2 + [\mathrm{Im}(u_1)]^2} \\ |u_2| = \sqrt{[\mathrm{Re}(u_2)]^2 + [\mathrm{Im}(u_2)]^2} \end{cases}, \tag{35}$$

where Re(·) and Im(·) are the real and image part of a complex expression, respectively.

It is convenient to define the dimensionless frequency (or dimensionless wavenumber) η as the ratio of the maximum width of the valley to the incident wavelength λ_1, that is,

$$\eta = \frac{\omega a}{\pi c_1} = \frac{k_1 a}{\pi} = \frac{2a}{\lambda_1}. \tag{36}$$

All computer codes for this paper have been implemented entirely in the Mathematica 5.2 programming environment (Wolfram 2003), which offers direct support for arbitrary precision arithmetic.

3 NUMERICAL RESULTS AND DISCUSSIONS

3.1 Frequency-domain responses

In this subsection, the authors focus on a 'soft' alluvial valley. The physical parameters corresponding to the material properties are set as follows: the mass density ratio ρ_1/ρ_2 was fixed at 1.5, and the shear wave velocity ratio c_1/c_2 was chosen as 2.0, 2.5 or 3.0. These values were based on the works of Trifunac (1971) and Kawase & Aki (1989) for the Mexico City valley.

A convergence test was done to specify the truncation limit for the infinite series in eqs (24) and (25). It was worth emphasizing that the M terms of summation should be accurately computed by numerically testing for their convergence, thereby leaving only one parameter to eliminate the phenomenon of relative convergence in the numerical procedure, that is, the N terms of summation.

In order to verify that the infinite series involved in the solution is convergent, two examples of dimensionless alluvium thickness $h/a = 0.25$ and 0.75 at horizontal incidence ($\alpha = 90^\circ$) for the dimensionless frequency $\eta = 2.0$ are considered in Fig. 2. The shear wave velocity ratio c_1/c_2 is 2.0. The primary reason for choosing the horizontal incidence case is that it needs more terms than any other case of incidence. These two examples show the variation of surface displacement amplitudes with the truncated number N of the infinite series. The plotted range of the dimensionless distance x/a is from -4 to 4, and the range of x/a from -1 to 1 corresponds to the horizontal position of the valley surface.

As seen in Fig. 2, the convergence is achieved after $N = 8$. This is relatively a small number of terms required to achieve convergence. Numerical tests also showed that more terms were required as the dimensionless frequency η increased. Besides, to guarantee a given computational precision, $M = 50$ terms in eqs (24) and (25) were chosen to produce the graphs in all following cases.

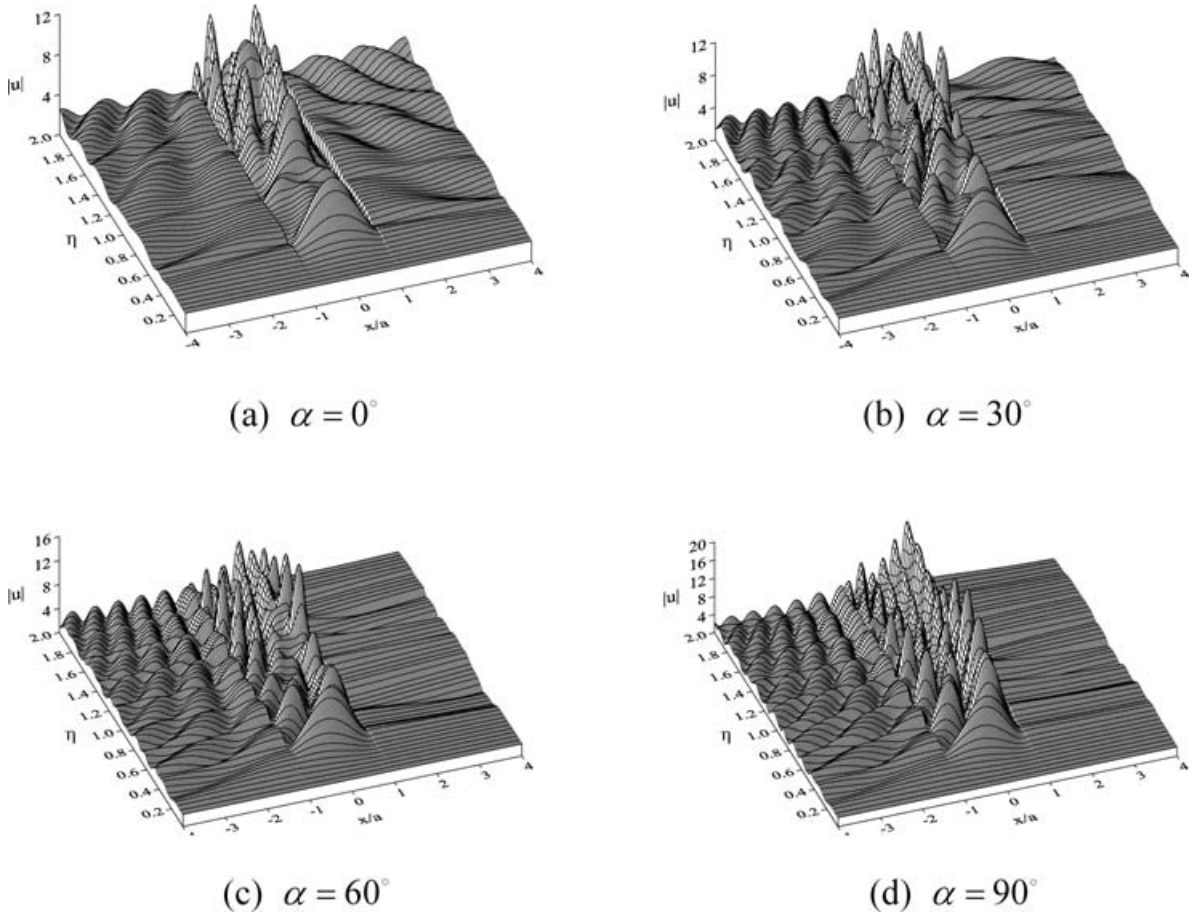

Figure 8. 3-D plots of surface displacement amplitudes for different α at $\rho_1/\rho_2 = 1.5$, $c_1/c_2 = 2.0$ and $h/a = 0.75$.

To demonstrate the effects of the dimensionless alluvium thickness h/a on the displacement amplitude $|u|$, three groups of results for $h/a = 0.25$, 0.5, 0.75 and 1.0 are calculated at different incident angles ($\alpha = 0^\circ$, 30°, 60° and 90°) with shear wave velocity ratio $c_1/c_2 = 2.0$. The first group corresponding to the dimensionless frequency $\eta = 0.5$ is illustrated in Fig. 3, while the second one corresponding to the dimensionless frequency $\eta = 1.0$ is shown in Fig. 4. For the third group in Fig. 5, the dimensionless frequency η is considered to be 2.0.

From a low frequency ($\eta = 0.5$) case in Fig. 3, it shows that, for the partially filled case ($h/a < 1.0$), the value of the maximum response amplitude tends to increase with increasing the alluvium thickness h/a. However, this increased trend does not include the completely filled alluvial valley ($h/a = 1.0$). That is to say, the peak amplitude for a partially filled case may be larger than that for a completely filled one. Such a difference is contrary to our original expectation. As to a fully filled alluvial valley, it was commonly known in the past that an increase of valley depth causes the peak amplitude to be greater (see, e.g. Bard & Bouchon 1980). Now, if considering the depth of the alluvial valley as the thickness of the deposit, the above concept may no longer be fitting for the case of a partially filled alluvial valley.

As shown in Figs 4(a) and (b), one can observe that, at nearly vertical incidences ($\alpha = 0^\circ$ and 30°) with moderate frequency ($\eta = 1.0$), the maximum amplitudes of motions for a fully filled valley are much smaller than those for a lowly filled ($h/a = 0.25$) one. However, unlike the response at low or moderate frequency, Fig. 5 shows that at high frequency ($\eta = 2.0$) the variability of ground motions is very chaotic. The distribution of local peaks and depressions on the diagrams becomes denser with larger values of frequency. This may be explained by the fact that disturbance between the transmitted and rereflected wave inside the alluvial deposit is obviously getting stronger. On the other hand, the surface displacement appears to be sensitive upon the change of the alluvium thickness. This effect is very similar to the results of Dravinski (1982) who studied the influence of different interface depths of the alluvial valley on surface

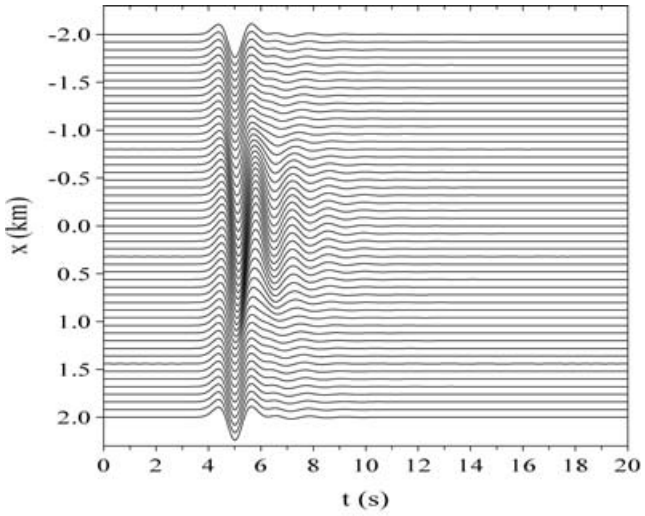

Figure 9. Synthetic seismograms for different h/a at $c_1/c_2 = 1.5$ and $\alpha = 0^\circ$.

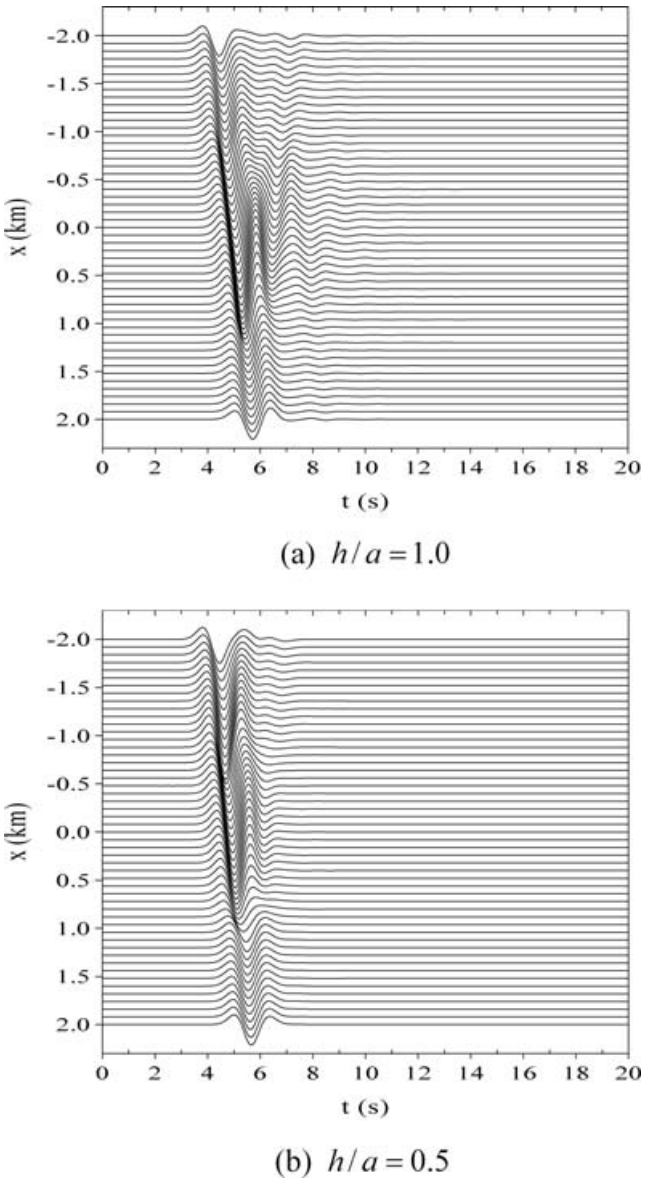

Figure 10. Synthetic seismograms for different h/a at $c_1/c_2 = 1.5$ and $\alpha = 60^\circ$.

motion. In addition, there is one thing to point out: at most incident angles the maximum value of displacement amplitudes for the fully filled valley ($h/a = 1.0$) are smaller than those for the highly filled ones ($h/a = 0.5$ and 0.75). For the reason of simplicity in Fig. 5, the curves for a fully filled case are not contained.

In comparing Figs 3–5, one can see that the patterns of displacement amplitudes for normal incidence ($\alpha = 0^\circ$) are symmetrical about the vertical axis. This is due to the symmetry of the valley about this axis. Overall, the displacement amplitudes in the illumination zone ($x/a < 1$) are more oscillatory and complicated than those in the shadow zone ($x/a > 1$) since the incident wave comes from the left side of the valley.

Subsequently, in order to obtain a clearer idea of effects of the velocity contrast on the response of a lowly filled ($h/a = 0.25$) valley, the changes in the displacement amplitudes with respect to the shear wave velocity ratio c_1/c_2 are plotted in Fig. 6. The dimensionless frequency η is 1.0. It can be seen that the value of the maximum response amplitude increases with increasing value of the shear wave velocity ratio c_1/c_2 except the vertical incidence case ($\alpha = 0^\circ$).

Figs 7 and 8 illustrate the displacement amplitudes as a function of the dimensionless distance x/a and the dimensionless frequency η at various angles of incidence ($\alpha = 0^\circ$, 30°, 60° and 90°). The former corresponds to the dimensionless alluvium thickness $h/a = 0.25$, while the latter corresponds to the case of $h/a = 0.75$. The shear wave velocity ratio c_1/c_2 is 2.0. As seen in Figs 7 and 8, they give a good portrait of the frequency behaviour of the ground surface motion. The resonant behaviour is sometimes clear when several peaks are distributed in space for a given frequency. It is apparent that the displacement amplitude patterns on the range of $-1 \leq x/a \leq 1$ for a highly filled alluvial valley are more complex than those for a lowly filled one.

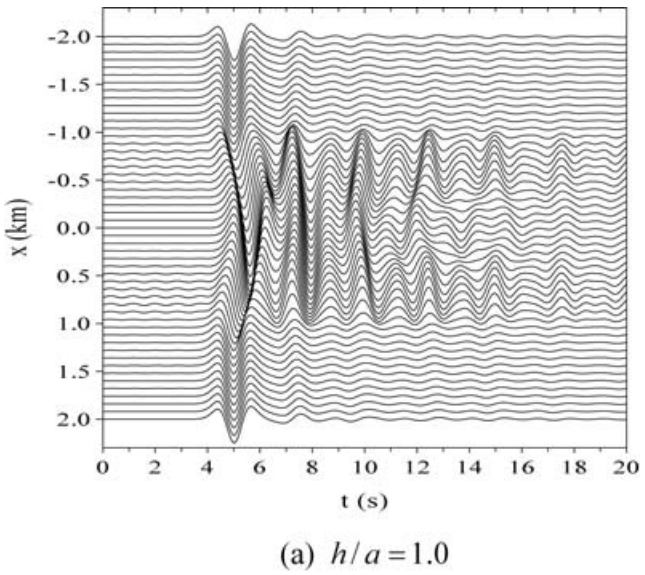

Figure 11. Synthetic seismograms for different h/a at $c_1/c_2 = 3.0$ and $\alpha = 0^\circ$.

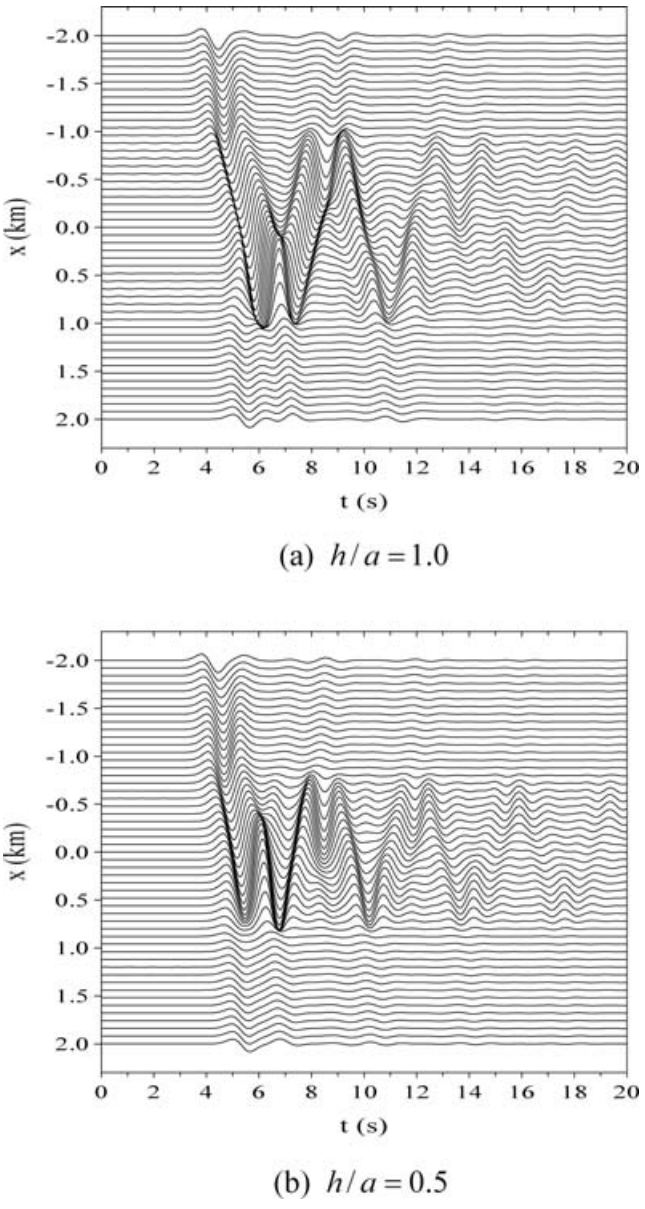

Figure 12. Synthetic seismograms for different h/a at $c_1/c_2 = 3.0$ and $\alpha = 60^\circ$.

3.2 Time-domain responses

Here, the model response in the time-domain is obtained from the frequency domain solution using Fast Fourier Transform technique. The incident signal, a symmetric Ricker wavelet (e.g. previously used by Bard & Bouchon 1980) is taken and defined as

$$f(t) = \frac{\sqrt{\pi}}{2}\left[\frac{\pi^2(t-t_s)^2}{t_p^2} - \frac{1}{2}\right]\exp\left[-\frac{\pi^2(t-t_s)^2}{t_p^2}\right], \qquad (37)$$

where t_s corresponds to the arrival time of the peak amplitude of the wavelet and t_p corresponds to the characteristic period. In the following cases, most parameter settings are referred to the work of Luzón *et al.* (2004). The Ricker parameters are selected at $t_p = 1.6$ s and $t_s = 5$ s. The calculated frequencies are 128 in total, ranging from 0.0 to 2.0 Hz. 51 equally spaced stations are located along the ground and valley surface (from $x = -2$ km up to $x = 2$ km). The radius of the valley is equal to 1 km. The mass density ratio ρ_1/ρ_2 is fixed at 1.5. The shear wave velocity of the half-space c_1 is chosen as 3 km s^{-1}.

The time-series of the fully filled ($h/a = 1.0$) and partially filled ($h/a = 0.5$) alluvial valley with the shear wave velocity ratio $c_1/c_2 = 1.5$ at vertical ($\alpha = 0^\circ$) and nearly horizontal ($\alpha = 60^\circ$) incidence are plotted in Figs 9 and 10. In Figs 11 and 12, the shear wave velocity ratio c_1/c_2 is changed to 3.0, and other parameters are kept the same.

As expected, larger impedance contrast produces longer duration of the response. This is due to the fact that, for the lower impedance contrast cases, most of wave energy is transmitted back into the half-space. Oppositely, for the higher impedance contrast cases, a sizable part of the energy is trapped inside the valley.

From Figs 11 and 12, one can obviously found that the amplification zone for a fully filled valley is broader than that for a partially filled one. The same feature can be slightly found in Figs 9 and 10.

4 CONCLUSION

A novel application of the region-matching technique in connection with Graf's addition theorem to the half-space scattering problem of plane SH waves has been proposed. A series solution for the case of a partially filled semi-circular alluvial valley has been completely derived. Numerical results based on these series solutions have been calculated and discussed. These new solutions are intrinsically important because they not only enrich the list of geometries of alluvial valleys, but also provide challenging criteria for the validation of numerical frequency- and time-domain codes. Besides, other more general types of the partially filled semi-circular alluvial valleys will constitute the topics of investigations, and their series solutions may be developed in the future through the present theoretical treatment.

ACKNOWLEDGMENTS

We thank the Editor, Prof Jean Virieux and two anonymous referees for their encouragements on our manuscript, and for the reviewers' constructive corrections and suggestions helped to improve the quality of this work significantly.

REFERENCES

Abramowitz, M. & Stegun, I.A., 1972. *Handbook of Mathematical Functions, with Formulas, Graphs, and Mathematical Tables*, Dover, New York.

Bard, P.-Y. & Bouchon, M., 1980. The seismic response of sediment-filled valleys. Part 1: the case of incident SH waves, *Bull. Seism. Soc. Am.,* **70**(4), 1263–1286.

Bielak, J., MacCamy, R.C., McGhee, D.S. & Barry, A., 1991. Unified symmetric BEM-FEM for site effects on ground motion—SH waves, *J. Eng. Mech., ASCE,* **117**(10), 2265–2285.

Bielak, J., Xu, J. & Ghattas, O., 1999. Earthquake ground motion and structural response in alluvial valleys, *J. Geotech. Geoenviron. Eng., ASCE,* **125**(5), 413–423.

Boore, D.M., 1972. Finite difference methods for seismic wave propagation in heterogeneous materials, in *Methods in Computational Physics,* Vol. 11, pp. 1–37, ed. Bolt, B.A., Academic Press, New York.

Bouchon, M., Campillo, M. & Gaffet, F., 1989. A boundary integral equation—discrete wavenumber representation method to study wave propagation in multilayered media having irregular interfaces, *Geophysics,* **54**(9), 1134–1140.

Dravinski, M., 1982. Influence of interface depth upon strong ground motion, *Bull. Seism. Soc. Am.,* **72**(2), 597–614.

Fishman, K.L. & Ahmad, S., 1995. Seismic response for alluvial valleys subjected to SH, P, and SV waves, *Soil Dyn. Earthq. Eng.,* **14**(4), 249–258.

Gil-Zepeda, S.A., Montalvo-Arrieta, J.C., Vai, R. & Sánchez-Sesma, F.J., 2003. A hybrid indirect boundary element—discrete wave number method applied to simulate the seismic response of stratified alluvial valleys, *Soil Dyn. Earthq. Eng.,* **23**(2), 77–86.

Hudson, D.E., 1972. Local distribution of strong earthquake ground motions, *Bull. seism. Soc. Am.,* **62**(6), 1765–1786.

Kawase, H. & Aki, K., 1989. A study on the response of a soft basin for incident S, P, and Rayleigh waves with special reference to the long duration observed in Mexico City, *Bull. seism. Soc. Am.,* **79**(5), 1361–1382.

King, J.L. & Tucker, B.E., 1984. Observed variations of earthquake motion across a sediment-filled valley, *Bull. seism. Soc. Am.,* **74**(1), 137–151.

Luzón, F., Ramírez, L., Sánchez-Sesma, F.J. & Posadas, A., 2004. Simulation of the seismic response of sedimentary basins with vertical constant-gradient velocity for incident SH waves, *Pure appl. Geophys.,* **161,** 1533–1547.

Lysmer, J. & Drake, L.A., 1972. A finite element method for seismology, in *Methods in Computational Physics,* Vol. 11, pp. 181–216, ed. Bolt, B.A., Academic Press, New York.

Pao, Y.-H. & Mow, C.C., 1973. *Diffraction of Elastic Waves and Dynamics Stress Concentrations,* Crane Russak, New York.

Papageorgiou, A.S. & Kim, J., 1991. Study of the propagation and amplification of seismic waves in Caracas valley with reference to the 29 July 1967earthquake: SH waves, *Bull. seism. Soc. Am.,* **81**(6), 2214–2233.

Sánchez-Sesma, F.J., Ramos-martínez, J. & Campillo, M., 1993. An indirect boundary element method applied to simulate the seismic response of alluvial valleys for incident P, S and Rayleigh waves, *Earthq. Eng. Struct. Dyn.,* **22,** 279–295.

Smith, W.D., 1975. The application of finite element analysis to body wave propagation problems, *Geophys. J. R. Astr. Soc.,* **42,** 747–768.

Trifunac, M.D., 1971. Surface motion of a semi-cylindrical alluvial valley for incident plane SH waves, *Bull. seism. Soc. Am.,* **61**(6), 1755–1770.

Trifunac, M.D., 1973. Scattering of plane SH waves by a semi-cylindrical canyon, *Earthq. Eng. Struct. Dyn.,* **1,** 267–281.

Tucker, B.E. & King, J.L., 1984. Dependence of sediment-filled valley response on input amplitude and valley properties, *Bull. seism. Soc. Am.,* **74**(1), 153–165.

Watson, G.N., 1958. *A Treatise on the Theory of Bessel Functions,* 2nd edn, Cambridge, England.

Wolfram, S., 2003. *The Mathematica Book,* 5th edn, Wolfram Media, Champaign, IL, USA.

Wong, H.L. & Trifunac, M.D., 1974. Surface motion of semi-elliptical alluvial valley for incident plane SH waves, *Bull. seism. Soc. Am.,* **64**(5), 1389–1408.